รูปแบบ **Abstract** (บทคัดย่อ)

Project Code : MRG56-0572
(รหัสโครงการ)

Project Title : แรงสัมผัสป้อนกลับในหุ่นยนต์ช่วยเหลือการทำงาน โดยการควบคุมความเร่งพร้อม
(ชื่อโครงการ) กับการชดเชยการรบกวนของกลไก

Investigator : อ. ดร. เชาวลิต มิตรสันติสุข มหาวิทยาลัยเกษตรศาสตร์
(ชื่อนักวิจัย)

E-mail Address : fengcrm@ku.ac.th, chowarit.ku@gmail.com

Project Period : 2 ปี
(ระยะเวลาโครงการ)

งานวิจัยฉบับนี้นำเสนอ การออกแบบตัวสังเกตการณ์สัญญาณรบกวนโดยใช้เซนเซอร์วัดความเร่ง และตัวกรองสัญญาณคาลมาลที่สามารถใช้ในการประมาณค่าแรงสัมผัสภายนอกที่ด้านฝั่งของภาระโหลดสำหรับระบบหลายมวล ตัวสังเกตการณ์สัญญาณรบกวนที่นำเสนอประยุกต์ใช้เซนเซอร์วัดความเร่ง และ เซนเซอร์วัดตำแหน่งด้วยวิธีการแสงในการวัดหาค่าแรงสัมผัส เนื่องจากเซนเซอร์วัดความเร่งสามารถติดตั้งไว้ในพื้นที่ขนาดเล็กที่ด้านปลายแขนของหุ่นยนต์ ทำให้วิธีการดังกล่าวนำไปใช้กับการใช้งานจริงได้อย่างเหมาะสม โดยการใช้ตัวสังเกตการณ์ที่นำเสนอไม่จำเป็นต้องประมาณหาค่าสัมประสิทธิ์ของระบบออกมาก่อน

ในระบบการควบคุมแรงโดยไม่จำเป็นต้องใช้เซนเซอร์วัดแรง ตัวสังเกตการณ์สัญญาณรบกวนสามารถนำมาใช้ร่วมกับการควบคุมอัตราส่วนการสั่นพ้อง เพื่อที่จะลดการสั่นจากความถี่สูงของสปริง เนื่องจากค่าตัวแปรของระบบควบคุมถูกออกแบบให้เหมาะสมโดยการใช้วิธีการแผนผังค่าสัมประสิทธิ์ การควบคุมอัตราการสั่นพ้องสามารถทำให้มั่นใจได้ว่าระบบควบคุมแรงสัมผัสมีสภาพทนทางที่ดี ค่าตัวแปรของการควบคุมอัตราการสั่นพ้องทั่งในระบบสองมวล และสามมวล ซึ่งแสดงในระบบกายภาพทั่วๆไปได้ถูกทำการวิเคราะห์โดยใช้วิธีที่ได้นำเสนอดังกล่าวนี้ นอกจากนี้วิธีการที่ได้นำเสนอยังสามารถนำไปประยุกต์ใช้กับระบบหลายมวลได้อีกด้วย ผลการทดลองประสิทธิภาพของระบบควบคุมในแง่ของการลดการสั่นสะเทือนนั้น มีผลลัพธ์ที่ดีออกมาสอดคล้องกับทฤษฎีและการจำลองด้วยสมการทางคณิตศาสตร์

Keywords : (คำหลัก) การประมาณค่าหาแรงสัมผัสภายนอก, ตัวกรองสัญญาณคาลมาล , ระบบหลายมวล, การสั่น

1 Introduction:

Robotic systems are being built to replace humans in the assistance of performing those repetitive and dangerous tasks which humans are unable to do. For example, industrial robot has been built to perform a task such as pick and place, welding, assembly, painting and product inspection. Robots can probably perform better than a human, because the robot can move more uniformly and more consistently. In the future development of robots, these robots are required to have an ability to accommodate the interaction potential with human operator.

Design of force controls to operate task while contacting with an unknown environments has been described in many papers. Several proposed techniques have paid attention to develop force control system and implemented force sensors to detect the external force. One problem of the using force sensor devices is that they are designed to contact the environment by using strain gauge at the end-effector. As a result, the vibration noise can occur significantly from the soft structure of the strain gauge. To improve the control performance, the observer technique is proposed to estimate the external force without force sensor. Many researches have involved this technique in order to reduce the complicity of the overall control system and increase their stability. Instead of relying on the detection of forces using force sensors, a disturbance observer is capable of estimating disturbance force information. It has been confirmed that efficiency of force estimation and robustness against disturbance can be improved at the same time by using disturbance observer as the feed forward compensation loop. The most important advantage of disturbance observer is that the force bandwidth can be enlarging much higher than the conventional force control with force sensor devices. Unfortunately the disturbance observer posed some challenges that remained unsolved. If such disturbance observer is to be used in a two-mass system with mechanical resonance, the instability and vibration effects can occur and degrade the overall performance. Usually, geared device is applied to increase the torque and reduces the speed of the robot's actuators. It can change the speed direction and torque conversions from the motor to another device. By using geared devices, the motor with gear system is considered as two mass systems. As a result, vibration effect from disturbance observer is occurred due to the mechanical resonance.

To address these problems, a load disturbance observer (LDOB) has been proposed to estimate load side external force by extracting vibration effects from the two-mass system. The structure of the observer is composed of the nominal spring coefficient, the nominal load mass and the encoder, which is attached at the load side. However, its main drawback is that the exact parameters of the spring coefficient are very difficult to obtain.

To get rid of possible parameter mismatch of spring coefficient, a multi encoder based disturbance observer (MEDOB) also provides solutions to estimate the external force at the load side. Since the position of the load side and disturbance force at the motor side can be obtained, parameters identification of spring coefficient is not required. However, its main drawback is that the encoder cannot be easily implemented at the load side due to the space/size limitation.

In this research, a new combined disturbance observer with Kalman filtering technique, named acceleration sensor based load side disturbance observer (ALDOB), has been proposed by using acceleration sensor at the load side and encoder at the motor side. Instead of using encoder to measure position response at the load side, an acceleration sensor is used to measure acceleration information from the end-effectors of the robot. Since acceleration sensors can be implemented in a small area on the load side, it is considered to be suitable for the real applications.

The compensation for vibration effect on the controller accuracy creates further design issues. Yuki et al. have developed a resonance ratio control that can be applied with a disturbance observer to compensate vibration effects in the position control. This idea is used later by Katsura et. al to design sensorless force controller. In this paper, the proposed ALDOB observer can be utilized with resonance ratio control to suppress high-frequency vibrations of spring. Since the optimal parameters are designed by using coefficient diagram method (CDM), the resonance ratio control can ensure good robustness of the force control. The parameters of resonance ratio control for two mass systems and three mass systems, which are representative of many physical systems, are also analyzed. Moreover, this proposed approach could also be applied for other multi mass system. From the simulation and experimental results, it is observed that the oscillations in the contact force response were small. The spring vibrations were significantly reduced in the contact force response.

2 Modeling of Flexible Robot System:

The systems of interest are the linear flexible structures that can be modeled using the two masses connected by a spring as shown in Fig. 1. Since the actuator is connected to the load side with a transmission mechanism, its elasticity causes resonance in the system. A block diagram of the linear motor with two-mass system that controls under the ideal current source is shown in Fig. 2. The equation of motion for such systems is given by:

$$\ddot{X}_M = -\frac{K_S}{M}X_S + \frac{K_T}{M}I_M, \quad (1)$$

$$\ddot{X}_L = \frac{K_S}{L}X_S - \frac{1}{L}F_L, \quad (2)$$

$$\dot{X}_S = \dot{X}_M - \dot{X}_L \quad (3)$$

where subscripts $_M$ and $_L$ denote the motor side and load side, respectively. K_S is the spring coefficient. F_S and F_L are the spring force and the external force on the load side. K_T is the force coefficient, I_M is the current, X_S is the torsional position from the position of the motor X_M and the position of the load X_L, M and L denote the equivalent mass of the linear motor and load mass,

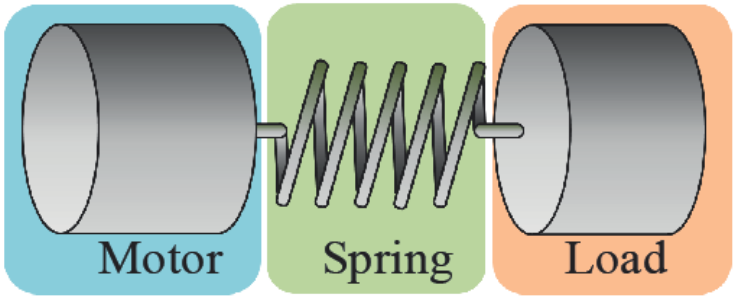

Fig. 1. Modeling of two mass system.

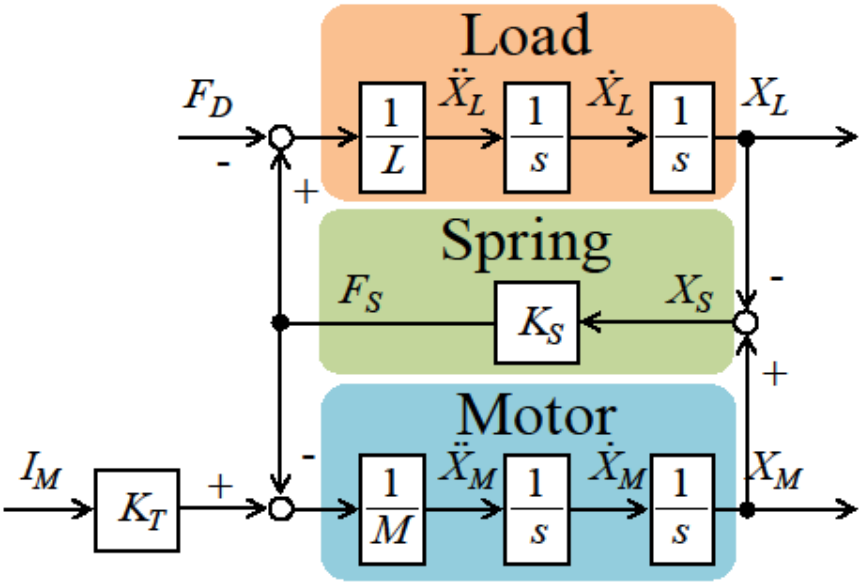

Fig. 2. The block diagram of two mass system.

respectively. Naturally, this flexible transmission can negatively affects the overall performance in terms of increased vibrations.

From Fig. 2, the transfer function from current reference I_M to the velocity of motor side $\dot{X}_M$ and the transfer function from current reference I_M to the velocity of load side $\dot{X}_L$ can be calculated as follows,

$$\frac{\dot{X}_M}{I_M} = \frac{\frac{K_T}{M}(s^2+\frac{K_S}{L})}{s^3+(\frac{K_S}{L}+\frac{K_S}{M})s}, \quad (4)$$

$$\frac{\dot{X}_L}{I_M} = \frac{\frac{K_T K_s}{ML}}{s^3+(\frac{K_S}{L}+\frac{K_S}{M})s}. \quad (5)$$

Then, the anti-resonance ω_{AR} and resonance frequencies ω_{R} can be described as follows,

$$\omega_R = \sqrt{\frac{K_S}{L}+\frac{K_S}{M}}, \quad (6)$$

$$\omega_{AR} = \sqrt{\frac{K_S}{L}}. \quad (7)$$

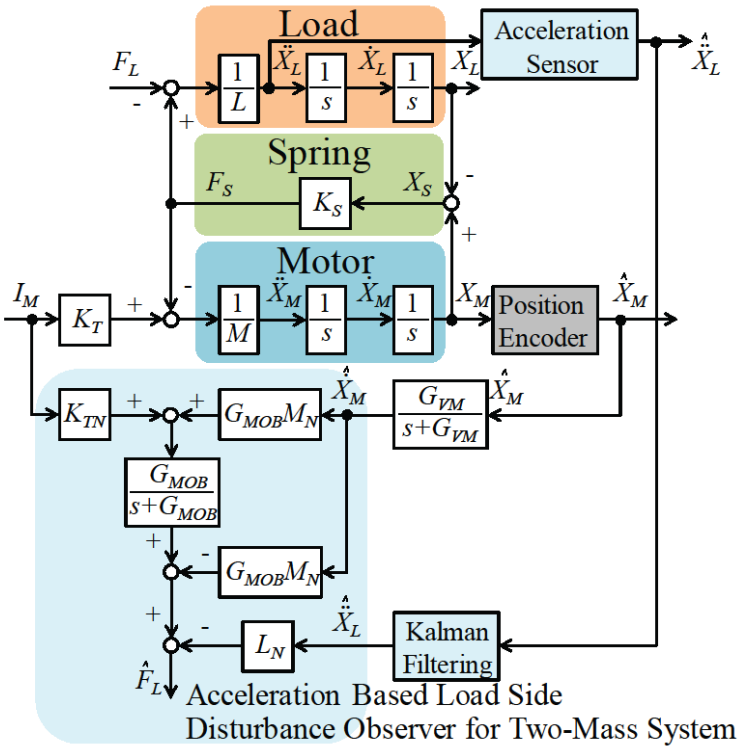

Fig. 3. Schematic diagram of Acceleration Sensor based Load Side Disturbance Observer for two mass system

3 Observer Based External Force Estimation:

One problem of the using force sensor devices is that they are designed to contact the environment by using strain gauge at the end-effector. As a result, the vibration noise can occur significantly from the soft structure of the strain gauge. To improve the control performance, the observer technique is proposed to estimate the external force without force sensor.

Acceleration Sensor based Load Side Disturbance Observer (ALDOB)

3.1 ALDOB for Two mass system

In this research, a new combined observer technique, named acceleration sensor based load side disturbance observer (ALDOB), has been proposed by using acceleration sensor and optical encoder. Applying an acceleration sensor scheme is an alternative way to supply the movement information of load side to a disturbance observer. Instead of using optical encoder to measure position response at the load side, an acceleration sensor is used to measure acceleration information from the end-effectors. Since acceleration sensors can be implemented in a small area on the load side, it is considered to be suitable for the real applications. The method to estimate the external force at the load side is obtained from the Kalman filter, disturbance observer and a simple first-order low-pass filter as follows,

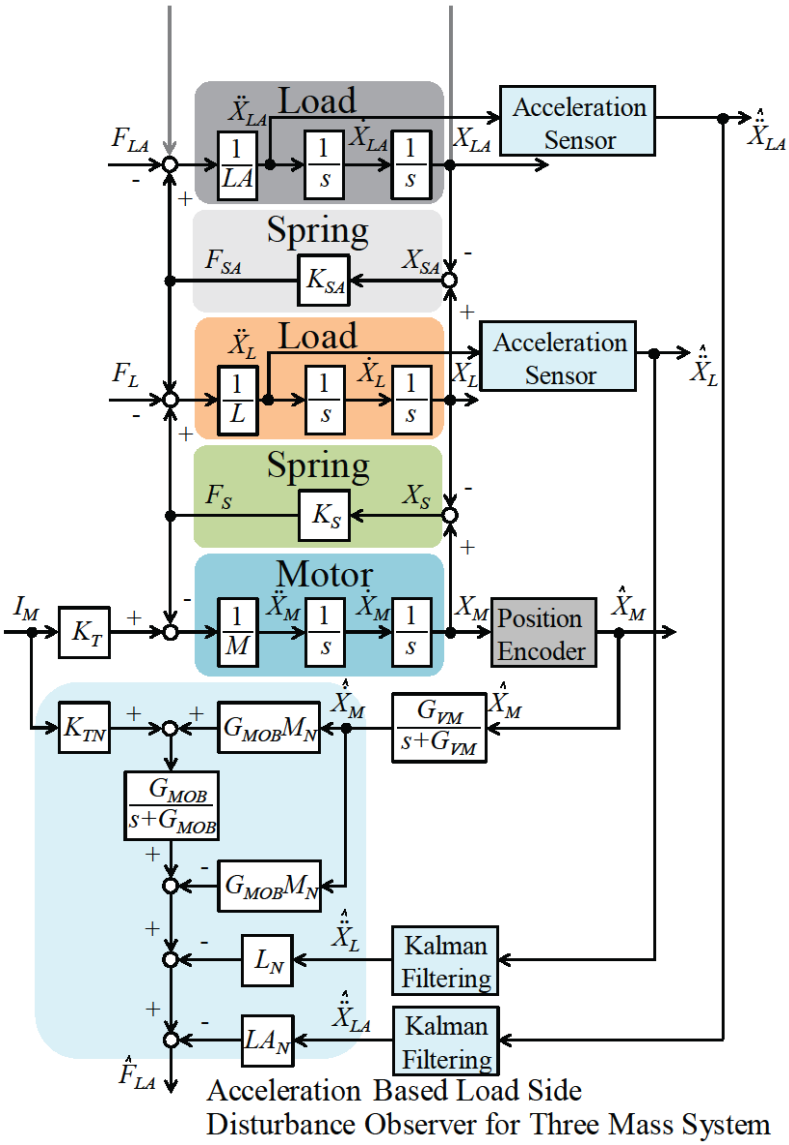

Fig. 4. Schematic diagram of Acceleration Sensor based Load Side Disturbance Observer for three mass system

$$\hat{F}_L = \left(\frac{G_{MOB}}{s+G_{MOB}}\left(K_{TN}I_M + G_{MOB}M_N\hat{\dot{X}}_M\right) - G_{MOB}M_N\hat{\dot{X}}_M - L_N\hat{\ddot{X}}_L\right) \quad (8)$$

where K_{TN} and M_N are refer to the nominal force coefficient and the nominal motor mass, respectively. $\dot{X}_M$ is the velocity of motor side. G_{MOB} is the cut-off frequency of the observer; L_N and $\ddot{X}_L$ are the nominal load mass and the acceleration of load side, respectively.

3.2 ALDOB for Three mass system

Such techniques can also apply in the flexible robot based on multi-mass system as shown in Fig. 4. In this section, a specially designed of acceleration based load-side disturbance observer that can be used to estimate the external force of multi-mass system is analyzed. The dynamic equation of the upper part of three-mass system is described by,

$$\ddot{X}_{L_A} = \frac{K_{SA}}{L_A} X_{SA} - \frac{1}{LA} F_{L_A}, \quad (9)$$

$$\dot{X}_{SA} = \dot{X}_L - \dot{X}_{L_A} \quad (10)$$

where A denotes the parameters of the third mass.

The total external force on the load side F_{LA} without the vibration effect can be estimated as

$$F_{L_A} = K_{TN} I_M - M_N \ddot{X}_M - L_N \ddot{X}_L - L_{AN} \ddot{X}_{L_A} \quad (11)$$

$$\hat{F}_{L_A} = \left(\frac{G_{MOB}}{s + G_{MOB}} \left(K_{TN} I_M + G_{MOB} M_N \hat{\dot{X}}_M \right) - G_{MOB} M_N \hat{\dot{X}}_M - L_N \hat{\ddot{X}}_L - L_{AN} \hat{\ddot{X}}_{L_A} \right) \quad (12)$$

As shown in Fig. 3 and 4, the Kalman-filter is applied to compensate the unwanted white Gaussian noise of the acceleration signal. The process of the Kalman-filter consisting of the operation in two phases: prediction and update. Using a Kalman filter, the state-space formulation of the measured acceleration signal can be expressed as

$$\boldsymbol{x}_{(k+1)} = \boldsymbol{A}_{(k)} \boldsymbol{x}_{(k)} + \boldsymbol{B}_{(k)} \boldsymbol{u}_{(k)} + \boldsymbol{w}_{(k)} \quad (13)$$

$$\boldsymbol{z}_{(k)} = \boldsymbol{C}_{(k)} \boldsymbol{x}_{(k)} + \boldsymbol{v}_{(k)} \quad (14)$$

where k represents the sampling instant, $x_{(k)}$ is the vector of states, $u_{(k)}$ is the vector of input variables, $A_{(k)}$ and $B_{(k)}$ are system matrices, $C_{(k)}$ is the measurement matrix, $z_{(k)}$ is the vector of measured variables, $w_{(k)}$ is the process noise and $v_{(k)}$ represents the measurement which is corrupted by white Gaussian noise. It is assumed that the covariance matrix of the process Q, the covariance matrices of the measurement noise R and the cross-covariance matrix are as given below:

$$\boldsymbol{Q} = E\{ww^T\} > 0 \quad (15)$$

$$\boldsymbol{R} = E\{vv^T\} \geqslant 0 \quad (16)$$

$$E\{wv^T\} = 0 \quad (17)$$

The matrices Q and R are used to tune the accuracy and response of the observer, and these values can be determined by using the simulations for the testing of the measurement sensors. A compromise between the performance of observer and the compensation of acceleration signal noise can be found. The Kalman filter estimation and updating equations for signal enhancement are as follows:

$$\boldsymbol{x}_{(k|k-1)} = \boldsymbol{A}_{(k-1)} \boldsymbol{x}_{(k-1|k-1)} + \boldsymbol{B}_{(k-1)} \boldsymbol{u}_{(k-1)} \quad (18)$$

$$\boldsymbol{P}_{(k|k-1)} = \boldsymbol{A}_{(k-1)} \boldsymbol{P}_{(k-1|k-1)} \boldsymbol{A}^T_{(k-1)} + \boldsymbol{Q}_{(k-1)} \quad (19)$$

$$\boldsymbol{S}_{(k)} = \boldsymbol{C}_{(k)} \boldsymbol{P}_{(k|k-1)} \boldsymbol{C}^T_{(k)} + \boldsymbol{R}_{(k)} \quad (20)$$

$$\boldsymbol{M}_{(k)} = \boldsymbol{P}_{(k|k-1)} \boldsymbol{C}^T_{(k)} \boldsymbol{S}^{-1}_{(k)} \quad (21)$$

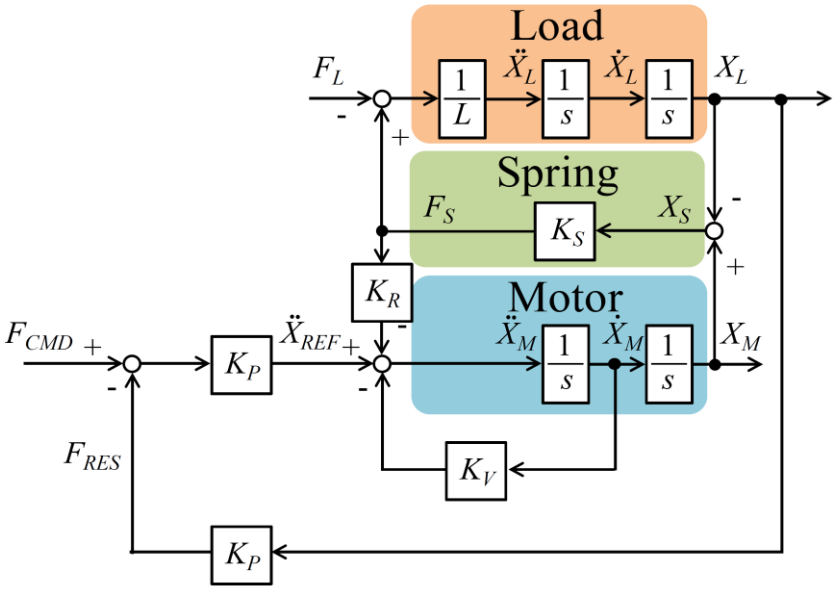

Fig. 5. The simplified block diagram of the resonance ratio control for two mass system

$$\boldsymbol{x}_{(k|k)} = \boldsymbol{x}_{(k|k-1)} + \boldsymbol{M}_{(k)}(\bar{\boldsymbol{z}}_{(k)} - \boldsymbol{C}_{(k)}\boldsymbol{x}_{(k|k-1)}) \quad (22)$$

$$\boldsymbol{P}_{(k|k)} = \boldsymbol{P}_{(k|k-1)} - \boldsymbol{M}_{(k)}\boldsymbol{S}_{(k)}\boldsymbol{M}_{(k)}^{T} \quad (23)$$

where $\boldsymbol{P}$ is the error covariance matrices. $\boldsymbol{M}$ and $\boldsymbol{S}$ are the Kalman filter gain matrix and the total uncertainty measurement of matrix, respectively $\boldsymbol{z}_{(k)}$ is an actual measurement of acceleration sensor which is updated the estimated state vector and the error matrix at every sampling instan t.

4. Controller Design of Flexible Robot System

4.1 Resonance Ratio Control Based on CDM for Two-Mass System

In recent years, advances in motion control technologies have brought significant rapid growth to machine and robot development. A conventional PID controller exhibits good controlling ability and improvement on its output response. However, PID controller cannot perform well in the machine with vibration effects.

This leads to the development of more effective controller design to reduce the vibrat ion effects. Yuki et al. have developed a resonance ratio control that can be applied with disturbance observer to suppress the oscillation during task executions for a torsional vibration in the position control by feeding back the estimated reaction torque on the motor side. Thus, it is possible to change the resonance frequency of the system to an arbitrarily value. This idea is used later by Katsura et. al to design sensorless force controller.

The control structure design based on disturbance observer is less complex and more efficient as shown in Fig. 5. The force controller based on resonance ratio control consists of a force gain K_P, a velocity gain K_V and a reaction force gain K_R. The feedback force will depend on the force contact on the robot by known environment stiffness K_E.

From Fig. 5, the transfer functions from acceleration reference $\ddot{X}_{REF}$ to motor position X_M and motor position X_M to load position X_L can be calculated as follows,

$$\frac{\hat{X}_M}{\ddot{X}_{REF}} = \frac{Ls^2 + K_S}{Ls^4 + K_S(1 + K_R L)s^2} \quad (24)$$

$$\frac{\hat{X}_L}{\hat{X}_M} = \frac{K_S}{Ls^2 + K_S} \quad (25)$$

The new anti-resonance frequency ω_{AR} and the resonance frequency ω_R of the system can be computed as follows,

$$\omega_R = \sqrt{\frac{K_S}{L}(1 + K_R L)}, \quad (26)$$

$$\omega_{AR} = \sqrt{\frac{K_S}{L}}. \quad (27)$$

The transfer function of the force servoing based on resonance ratio control is given by,

$$\frac{F_{RES}}{F_{CMD}} = \frac{K_P K_E \omega_{AR}^2}{s^4 + K_V s^3 + \omega_R^2 s^2 + K_V \omega_{AR}^2 s + K_P K_E \omega_{AR}^2} \quad (28)$$

In this research, a new resonance ratio parameter is calculated by using the coefficient diagram method (CDM). The CDM design method is used to design the characteristic polynomial of the closed loop system by achieving a good balance of stability and good robust performance. As it is seen from equation (28), the coefficients of characteristic polynomial a_i are found as,

$$a_0 = K_P K_E \omega_{AR}^2 \quad (29)$$

$$a_1 = K_V \omega_{AR}^2 \quad (30)$$

$$a_2 = \omega_R^2 \quad (31)$$

$$a_3 = K_V \quad (32)$$

$$a_4 = 1.0 \quad (33)$$

The standard stability indices γ_i for the Manabe form are chosen as γ_1 =2.5, γ_2 =2.0, and γ_3 =2.0.

$$\tau = \frac{a_1}{a_0} = \frac{K_V}{K_P K_E} \quad (34)$$

$$\gamma_1 = \frac{a_1^2}{a_0 a_2} = \frac{K_V^2 \omega_{AR}^2}{K_P K_E \omega_R^2} = 2.5 \quad (35)$$

$$\gamma_2 = \frac{a_2^2}{a_1 a_3} = \frac{\omega_R^4}{K_V^2 \omega_{AR}^2} = 2.0 \quad (36)$$

$$\gamma_3 = \frac{a_3^2}{a_2 a_4} = \frac{K_V^2}{\omega_R^2} = 2.0 \quad (37)$$

Thus, the controller parameters calculated by the design of CDM are given as follow,

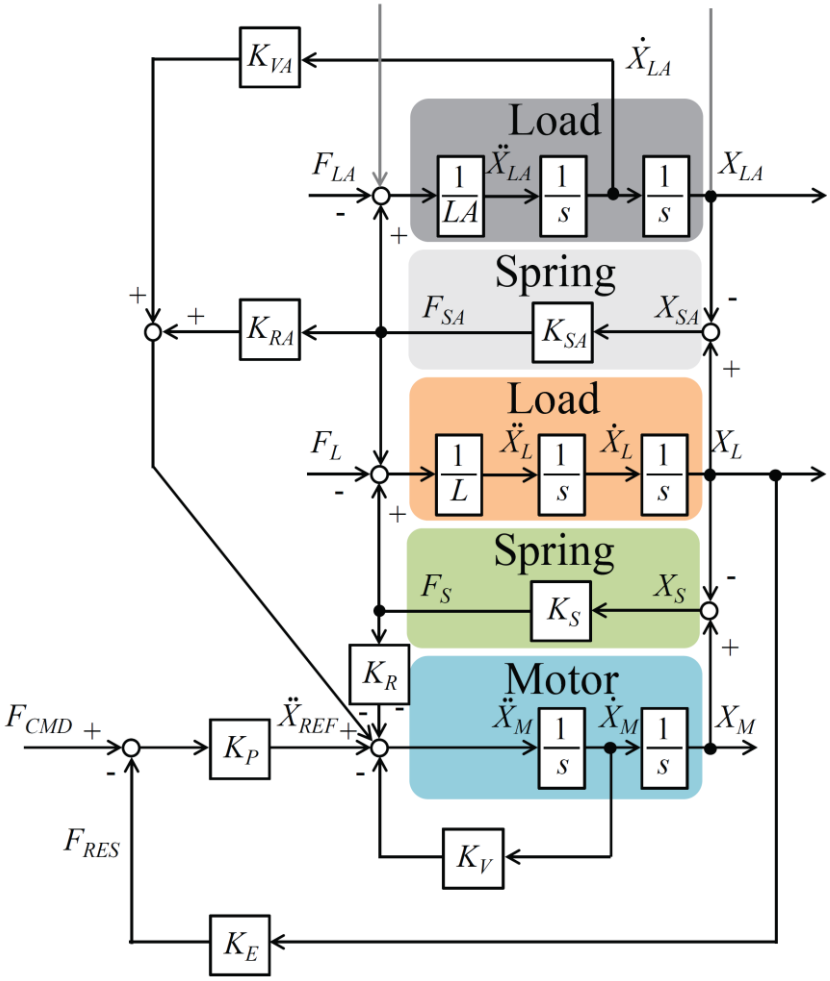

Fig. 6. The simplified block diagram of the resonance ratio control for three mass system

$$K_V = \sqrt{2}\omega_R \quad (38)$$

$$K_P = \frac{4\omega_{AR}^2}{5K_E} \quad (39)$$

$$K = \frac{\omega_R}{\omega_{AR}} = 2.0 \quad (40)$$

$$K_R = \frac{3}{L} \quad (41)$$

By setting these controller gains, a new resonance ratio parameter is chosen as 2.0.

4.2 Resonance Ratio Control Based on CDM for Three-Mass System

Similar control architecture can be implemented in the multi-mass system. The block diagram representation of a resonance ration control for three mass systems is shown in Fig. 6. If the acceleration signals are measured by sensors, the value of external torques or forces at the end-effector side can be determined by the ALDOB. Based on this principle, the external force from the load-side could be determined and compensated with a simple multiplication of the reaction force gain K_{RA} to the motor side. From the block diagram in Fig. 6, the transfer function of the three mass systems from the force command F_{CMD} to the motor displacement X_M can be expressed as

$$\frac{X_M}{F_{CMD}} = \frac{(s^2+\omega_{AR1}^2)(s^2+\omega_{AR2}^2)}{Ms^2(s^2+\omega_{R1}^2)(s^2+\omega_{R2}^2)} \quad (42)$$

where ω_{R1} and ω_{AR1} are the first resonance and anti-resonance frequency, and ω_{R2} and ω_{AR2} are the second resonance and anti-resonance frequency. The value of the ω_{AR1} and ω_{AR2} can be defined as the following calculation:

$$\omega_{AR1}^2 + \omega_{AR2}^2 = \frac{K_S + K_{SA}}{L} + \frac{K_{SA}}{L_A} \quad (43)$$

$$\omega_{AR1}^2 \omega_{AR2}^2 = \frac{K_S K_{SA}}{L L_A} \quad (44)$$

From the block diagram in Fig. 6, the transfer function of the three mass system from the force response F_{RES} to the force command F_{CMD} can be expressed as

$$\frac{F_{RES}}{F_{CMD}} = \frac{K_P K_E \omega_{AR1}^2 \omega_{AR2}^2}{a_6 s^6 + a_5 s^5 + a_4 s^4 + a_3 s^3 + a_2 s^2 + a_1 s + a_0} \quad (45)$$

The coefficients of characteristic polynomial a_i are found as,

$$a_0 = K_E K_P \omega_{AR1}^2 \omega_{AR2}^2 \quad (46)$$

$$a_1 = (K_V + K_{VA}) \omega_{AR1}^2 \omega_{AR2}^2 \quad (47)$$

$$a_2 = \omega_{AR1}^2 \omega_{AR2}^2 + (L + L_A) K_R \omega_{AR1}^2 \omega_{AR2}^2 + L_A K_{RA} \omega_{AR1}^2 \omega_{AR2}^2 \quad (48)$$

$$a_3 = K_V (\omega_{AR1}^2 + \omega_{AR2}^2) \quad (49)$$

$$a_4 = \omega_{AR1}^2 + \omega_{AR2}^2 + K_{SA} K_R \quad (50)$$

$$a_5 = K_V \quad (51)$$

$$a_6 = 1 \quad (52)$$

The standard stability indices γ_i for the Manabe form are chosen as γ_1 = 2.5, γ_2 =2.0, γ_3 =2.0, γ_4 = 2.0 and γ_5 =2.0.

$$\tau = \frac{a_1}{a_0} = \frac{K_V + K_{VA}}{K_P K_E} \quad (53)$$

$$\gamma_1 = \frac{a_1^2}{a_0 a_2} = \frac{(K_V + K_{VA})^2}{K_P K_E (1 + (L + L_A) K_R + L_A K_{RA})} = 2.5 \quad (54)$$

$$\gamma_2 = \frac{a_2^2}{a_1 a_3} = \frac{\omega_{AR1}^2 \omega_{AR2}^2 (1 + (L + L_A) K_R + L_A K_{RA})^2}{K_V (K_V + K_{VA})(\omega_{AR1}^2 + \omega_{AR2}^2)} = 2.0 \quad (55)$$

$$\begin{aligned}\gamma_3 &= \frac{a_3^2}{a_2 a_4} \\ &= \frac{K_V^2(\omega_{AR1}^2+\omega_{AR2}^2)}{\omega_{AR1}^2\omega_{AR2}^2(1+(L+L_A)K_R+L_AK_{RA})} \\ &\quad \times \frac{1}{(\omega_{AR1}^2+\omega_{AR2}^2+K_SK_R)} = 2.0\end{aligned} \tag{56}$$

$$\begin{aligned}\gamma_4 &= \frac{a_4^2}{a_3 a_5} \\ &= \frac{(\omega_{AR1}^2+\omega_{AR2}^2+K_SK_R)^2}{K_SK_R(\omega_{AR1}^2+\omega_{AR2}^2)} = 2.0\end{aligned} \tag{57}$$

$$\begin{aligned}\gamma_5 &= \frac{a_5^2}{a_4 a_6} \\ &= \frac{K_V^2}{\omega_{AR1}^2+\omega_{AR2}^2+K_SK_R} = 2.0\end{aligned} \tag{58}$$

Thus, the controller parameters calculated by the design of CDM are given as follow,

$$K_V = \sqrt{8(\omega_{AR1}^2+\omega_{AR2}^2)} \tag{60}$$

$$K_{VA} = \frac{\sqrt{8(\omega_{AR1}^2+\omega_{AR2}^2)}((\omega_{AR1}^2+\omega_{AR2}^2)^2-16\omega_{AR1}^2\omega_{AR2}^2)}{16\omega_{AR1}^2\omega_{AR2}^2} \tag{61}$$

$$K_R = \frac{3(\omega_{AR1}^2+\omega_{AR2}^2)}{K_S} \tag{62}$$

$$K_{RA} = \frac{K_S(\omega_{AR1}^2+\omega_{AR2}^2)-\omega_{AR1}^2\omega_{AR2}^2(K_S+3(L+L_A))}{K_S(L+L_A)\omega_{AR1}^2\omega_{AR2}^2} \tag{63}$$

$$K_P = \frac{LK_SA^2\sqrt{8A}}{40K_E(L_AK_S(A^2-B)+LB(K_S+3(LA-L_A)))} \tag{64}$$

where

$$A = \omega_{AR1}^2+\omega_{AR2}^2, B = \omega_{AR1}^2\omega_{AR2}^2 \tag{65}$$

5. Feedforward load disturbance compensation

5.1 Feedforward load disturbance compensation for two mass system

The block diagram of the proposed control structure is shown in Fig. 7. The load disturbance compensation is introduced to compute and feedback the estimated load disturbance force through the inverse system of the motor side. The inverse system can be represented by the transfer function from F_{CMD} to F_{RES} as shown in (45) and from F_L to F_{RES} as follows,

$$\frac{F_{RES}}{F_L} = \frac{\frac{1}{L}K_E(s^2+K_Vs+K_RK_S)}{s^4+K_Vs^3+\omega_R^2s^2+K_V\omega_{AR}^2s+K_PK_E\omega_{AR}^2} \tag{66}$$

Then, the inverse system can be calculated by the following equation:

$$\frac{F_{CMD}}{F_L} = \frac{s^2+K_Vs+K_RK_S}{K_PK_S} \tag{67}$$

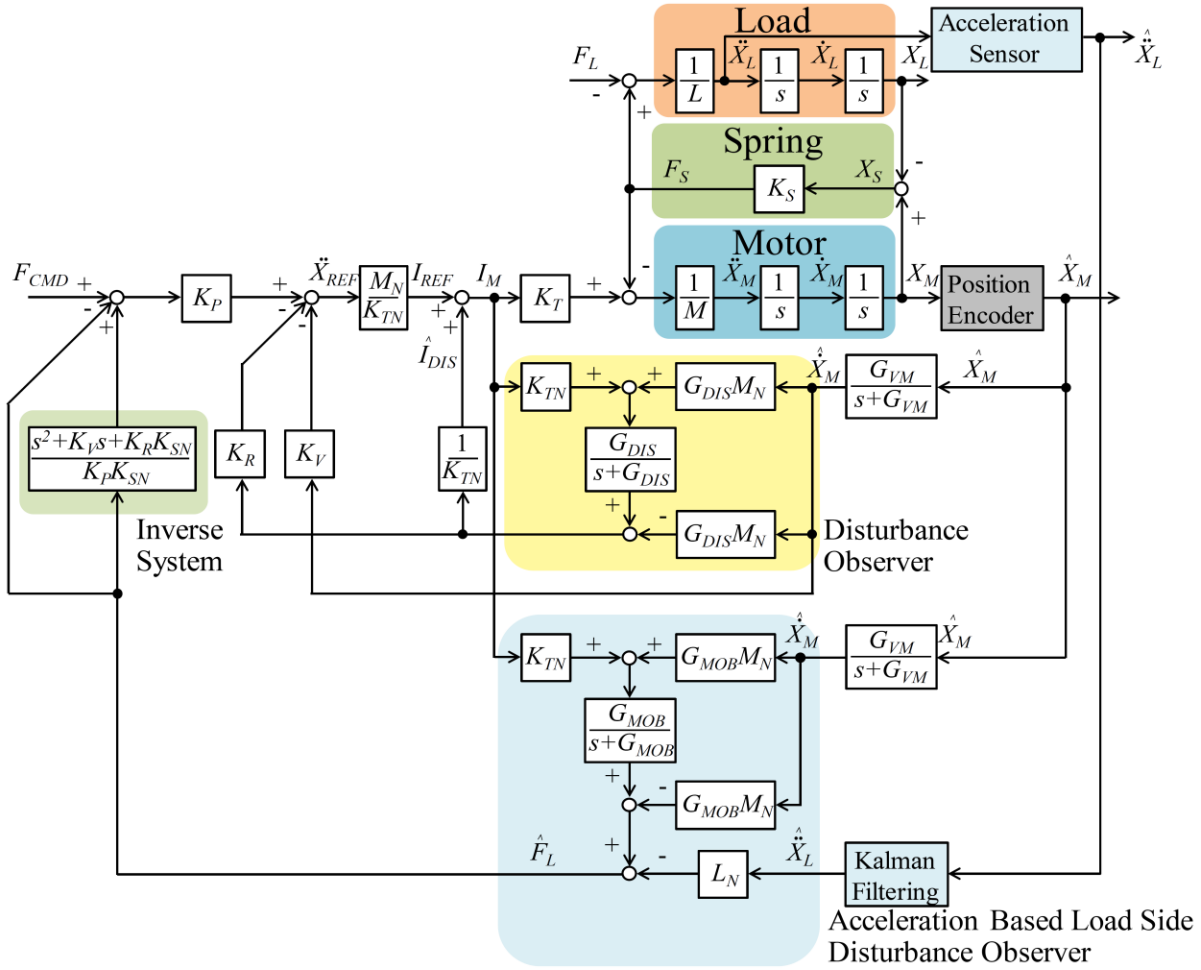

Fig. 7. The block diagram of the resonance ratio control based on ALDOB

5.2 Feedforward load disturbance compensation for three mass system

Using the same relationship as before, the transfer function relating force response F_{RES}, to the external force at the load side F_{LA}, for the three mass systems is

$$\frac{F_{RES}}{F_{LA}} = \frac{K_E(b_4 s^4 + b_3 s^3 + b_2 s^2 + b_1 s + b_0)}{a_6 s^6 + a_5 s^5 + a_4 s^4 + a_3 s^3 + a_2 s^2 + a_1 s + a_0} \tag{68}$$

where

$$\begin{aligned} b_0 &= (K_R + K_{RA}) K_S K_{SA}, b_1 = (K_S + K_{SA}) K_V \\ b_2 &= K_R K_S L + K_S + K_{SA}, b_3 = K_V L, b_4 = L \end{aligned}$$

Then, the feedforward load disturbance compensation for three mass systems can be expressed as

$$\frac{F_{CMD}}{F_L} = \frac{b_4 s^4 + b_3 s^3 + b_2 s^2 + b_1 s + b_0}{K_P K_S K_{SA}} \tag{69}$$

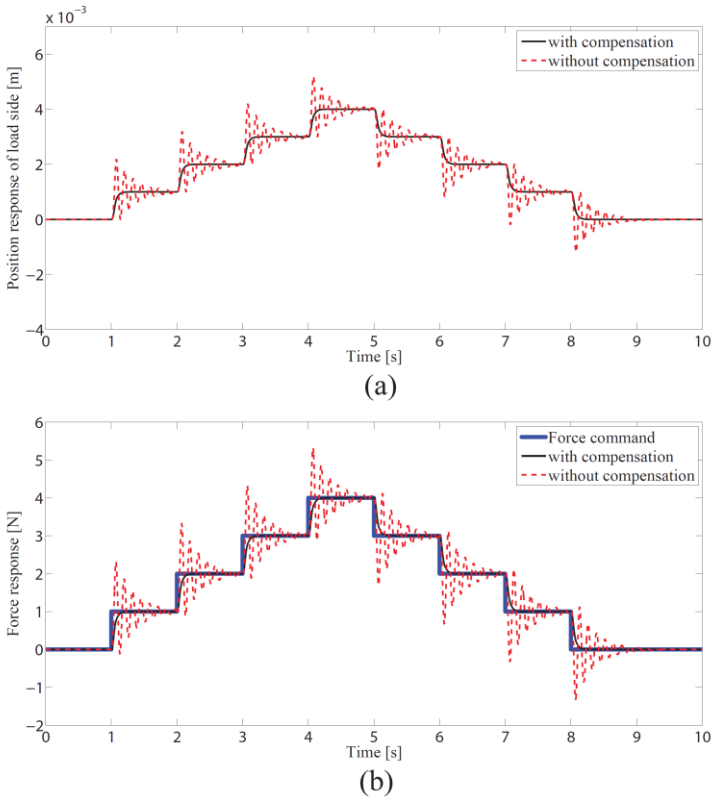

Fig. 8. Simulation results of two mass system.

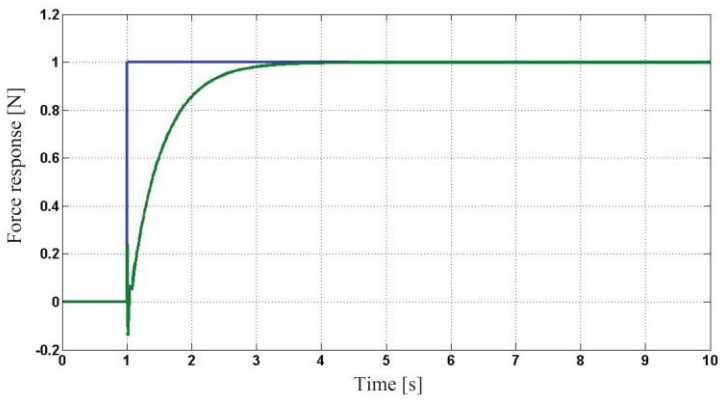

Fig. 9. Simulation results of three mass system.

For the flexible robot system having a multi mass, the proposed method can be applied and designed the controller and observer by calculating the transfer function of the multi mass system.

6. Simulation results

In order to show the validity and usefulness, numerical simulations are given to confirm of the proposed controller and observer design. The flexible robot system was simulated using MATLAB software. The results obtained from the proposed approach are compared with the results obtained from the conventional PID control. The first simulation result was conducted by using PID

TABLE I

PARAMETERS USED IN EXPERIMENTAL SETUP

Controller parameters	Symbol	Value	Units
Mass of motor	M	0.245	kg
Force constant coefficient	K_t	3.333	N/A
Mass of load	L	0.245	kg
Spring coefficient	K_{SN}	1100	N/m
Force gain	K_P	3.59	
Velocity gain	K_V	189.52	
Reaction force gain	K_R	12.24	
Resonance ratio gain	K	2	
Cut-off freq. of vel.	G_{VE}	1000	rad/s
Cut-off freq. of DOB.	G_{DIS}	1000	rad/s
Cut-off freq. of LDOB.	G_{LOB}	800	rad/s
Cut-off freq. of MEDOB.	G_{MOB}	800	rad/s

Table. 1. Parameters used in experimental setup.

controller, and the position, velocity, acceleration, and the contact force responses were collected as shown in Fig. 8. From the results, the force command input is a stepwise function. It is seen from Fig. 8 (b) that without reaction force compensation feedbacks give a poor response with a very large vibration. On the other hand, the vibration is well compensated in the case of the resonance ratio control. It is clear from these results that the resonance ratio control based on CDM design approach gives a good response with no overshoot and short settling time compared to the conventional PID controller design.

Extending from our proposed method, the resonance ratio control based on three mass systems was tested. The input step function is used as the force command. From Fig. 9, it is also confirmed that the resonance ratio control can compensate for vibration effect of the contact force response completely.

7. Experimental Results

This section describes experimental implementation of resonance ratio control using ALDOB in real conditions, and the contact force response, the speed and position of motor and load were being investigated. The control algorithm was implemented in a PC using RT-Linux with a sampling time of 100 μs. A summary of the parameters used in the experiment and the specification of sensors are presented in Table I and Table II, respectively. To verify the proposed observer and controller design of the flexible robot system, an acceleration sensor and linear optical encoder were implemented in the experimental feedback control system as shown in Fig. 10. The acceleration sensor was mounted on a linear motor at the load side, which has an optical encoder installed in order to observe vibration effect at the motor side and load side. The parameters in the controller were tuned to match the controller design in the identify transfer function of flexible robot system. All

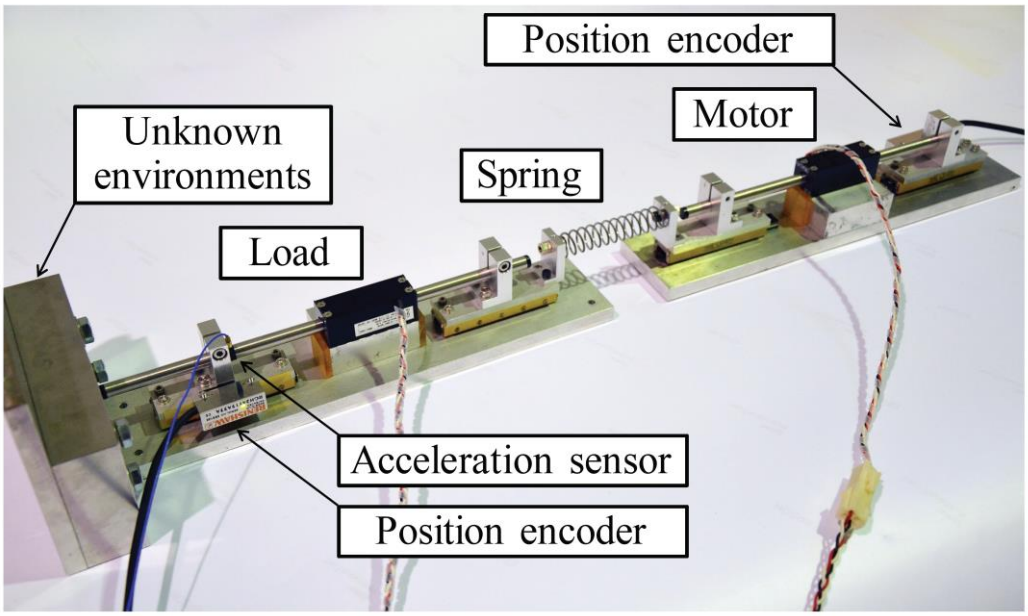

Fig. 10. Experimental setup of flexible robot system.

TABLE II

SPECIFICATION OF SENSORS

Optical encoder	Symbol	Value	Units
Resolution grade		0.1	μm
Weight		11.0	g
Dimension		14.8×36.0×13.5	mm
Maximum speed		10	m/s
Acceleration sensor	**Symbol**	**Value**	**Units**
Bandwidth		$1\sim10K$	Hz
Weight		5.0	g
Dimension		6.4×11.4×3.6	mm

Table. 2. Specification of sensors.

of the identified parameters were used to calculate the controller gain. The input stepwise is used as the force command. The control structure of resonance ratio control with a two-mass system as shown in Fig. 7 was investigated.

In the first experiment, a sponge was prepared as a sample environment for the test. On the other hand, an aluminum block was set at the end-effector in the second experiment. The aluminum block is usually stiffer than the sponge. It was embedded close to the end-effector of the robot. The responses of motor side and load side are shown in Figures 11 (a), (b) and 12 (a), (b) and the responses of the contact force estimation by using ALDOB and LDOB are shown in Fig. 11 (f) and 12 (f). Without the vibration compensation, it is found that the responses of position at the motor side and load side are oscillated. The influence of the reaction force feedback can be observed to

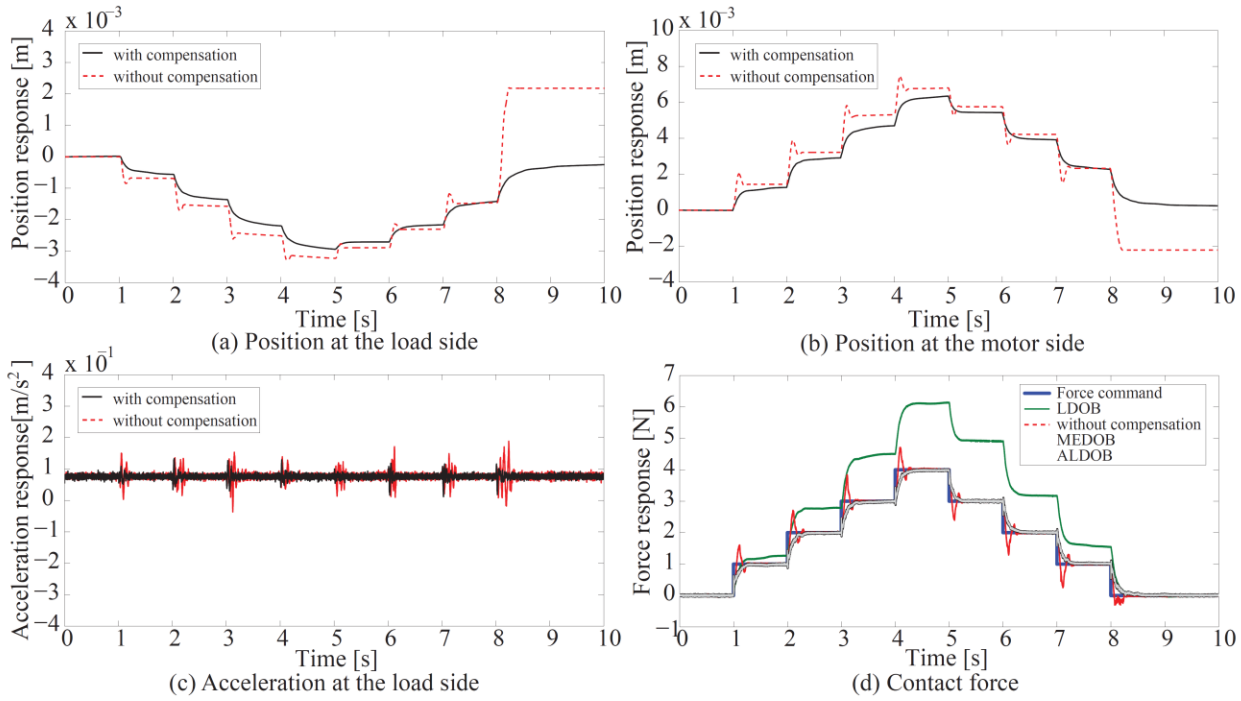

Fig. 11. Experimental results of linear motor in contact with a sponge.

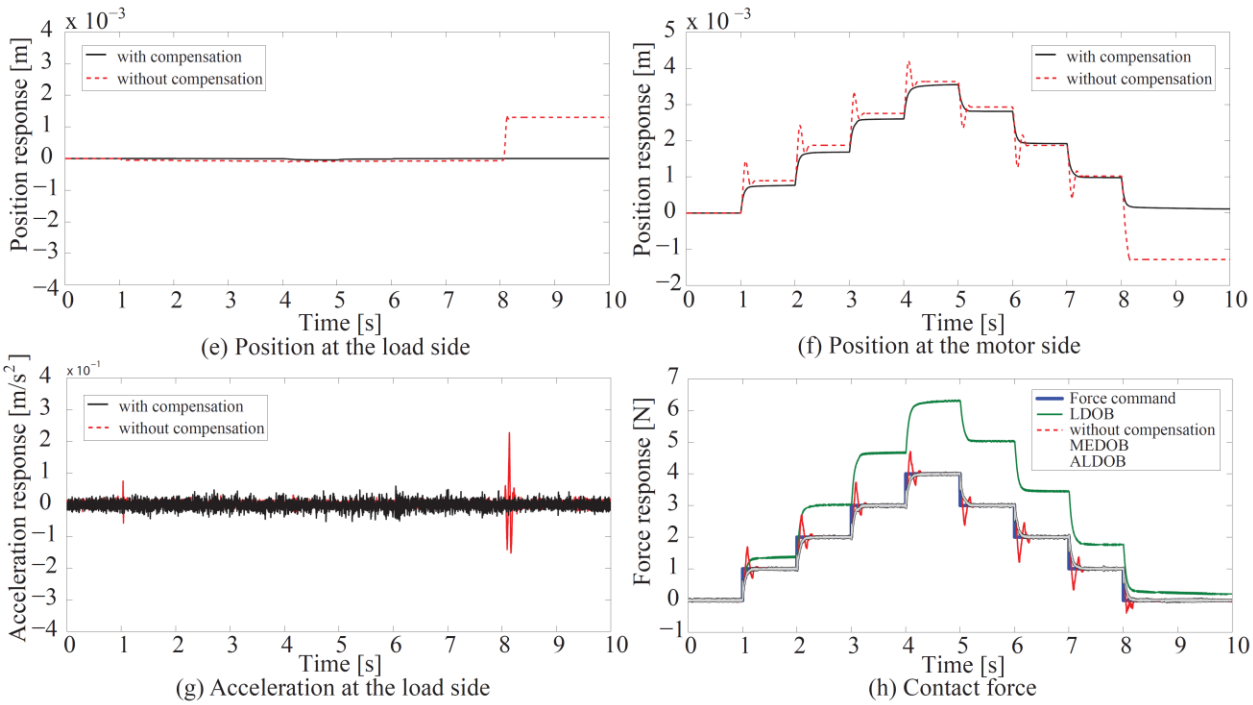

Fig. 12. Experimental results of linear motor in contact with an aluminum block.

significantly reduced the effective vibration by using the resonance ratio control. The improvement in the position and responses at the motor side and load side are illustrated. During the test, the contact force estimation using ALDOB were checked to confirm they matched the contact force estimation using MEDOB during experiments. By using LDOB, the mismatched value of the spring coefficient K_S caused incorrect estimation in the contact force response. If the spring coefficient is accurately identify, the force estimation can be improved the accuracy of the force estimation.

Figure 11 (f) and 12 (f) show the force response without and with compensator. The controller without the reaction force feedback compensation was chosen to illustrate the worst-case vibration. Based on the force estimation recorded during the test, the system force of the proposed method followed the reference command with only a small tracking error. By using the proposed resonance ratio control with ALDOB, it is observed that the oscillation in the contact force response were small. The spring vibrations were significantly reduced in the contact force response. It was shown that the resonance ratio control can suppress the oscillation more effectively than a conventional PID control.

8. Conclusion and future work

In this research, we described how acceleration sensor was integrated with ALDOB to estimate and control the contact force. Since acceleration sensors can be implemented in a small area on the load side, it is considered to be suitable for the real applications. The proposed ALDOB observer can be utilized with resonance ratio control to suppress high-frequency vibrations of spring. Since the optimal parameters are designed by using coefficient diagram method, the resonance ratio control can ensure good robustness of the force control. We performed this analysis for two types of systems, the two mass systems and three mass systems, which are representative of many physical systems. Moreover, this proposed approach could also be applied for other multi mass system. The obtained simulation and experimental results confirmed the efficiency of the proposed resonance ratio control with ALDOB for the robust force control system without use of force sensors.

9. Acknowledgment

The authors would like to thank Thailand Research Fund (TRF) for their support. This research was supported in part by a grant-in-aids from Thailand Research Fund (TRF).